RSC Advances

ROYAL SOCIETY OF CHEMISTRY

www.rsc.org/advances

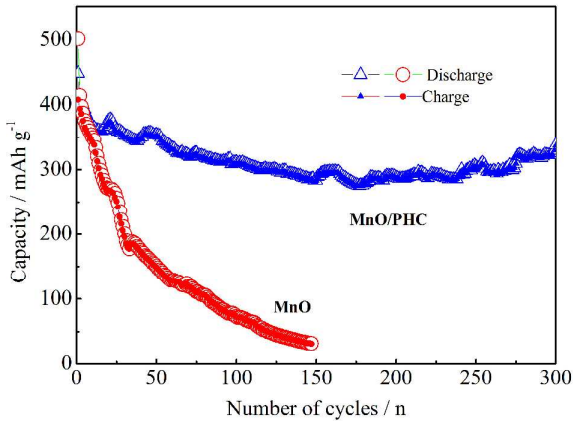

MnO/porous hard carbon nanocomposite as anode materials exhibits higher discharge/charge capability and good cycling performance at 2 C for 300 cycles.

Cite this: DOI: 10.1039/c0xx00000x

www.rsc.org/xxxxxx

ARTICLE TYPE

Novel MnO/conjugated microporous polymer derived-porous hard carbon nanocomposite for superior lithium storage

Qingtang Zhang,[a] Songwang Ge,[a] Xiaomei Wang,[b] Hanxue Sun,[a,b] Zhaoqi Zhu,[a] Weidong Liang[a] and An Li*[a]

Received (in XXX, XXX) Xth XXXXXXXXX 20XX, Accepted Xth XXXXXXXXX 20XX
DOI: 10.1039/b000000x

MnO/porous hard carbon (PHC) nanocomposite was prepared by thermolysis of the conjugated microporous polymer incorporated with $Mn(CH_3COO)_2$. The results obtained from scanning electron microscopy, transmission electron microscope and Brunauer–Emmett–Teller analysis show that MnO nano crystals are uniformly dispersed in the PHC matrix. The rate performance of MnO/PHC electrode at current rates over 5 C is remarkably higher than that of MnO electrode. After 200 charge/discharge cycles, the capacity retention ratio of MnO/PHC electrode still reaches up to 91.1%. Such unique performance of MnO/PHC nanocomposite makes it a promising candidate as anode materials for high performance lithium ion batteries.

Introduction

Lithium ion batteries (LIBs) have been attracted extensive attention in the past decades because of their intrinsic high energy density, high power density, and long cycling life. The construction of efficient electrode materials is essential to build advanced LIBs systems. Among those well-known anode materials, transition metal oxides (MO_x) have high reversible lithium storage (much higher than that of graphite ~372 mAh g^{-1}) based on the heterogeneous conversion reactions involved in the formation of transition metal nano-domains (M_0) dispersed in Li_2O matrix.[1] However, most of these conversion-type electrodes suffer from a large voltage hysteresis (higher than 1 V)[2] between charge and discharge process, resulting in poor energy efficiency. MnO was considered as one of the most excellent candidates among MO_x because it has relatively smaller voltage hysteresis (0.7 V). The average charge (delithiation) voltage of MnO is about 1.2 V[3-5] which is much lower than that of FeO (1.6 V)[1], CoO (1.8 V)[1], NiO (1.9 V)[6] and CuO (2.1 V)[7]. However, the main drawback of MnO lies in poor cyclic stability due to the pulverization and the loss of electronic contact of active particles as a consequence of large volume expansion/contraction associated with the lithium insertion/delithiation process. To address this issue, many approaches including decreasing particle size[4], MnO/C nanocomposite[8-9], coaxial MnO/C nanotubes[10], MnO/C core-shell nanorods[11] and MnO/Graphene[5, 12] have been applied to enhance and retain the conductivity of MnO during charge/discharge cycles. From a materials science standpoint, the development of novel strategy that can increase the conductivity of MnO and also make it well dispersed in carbon matrix should be of great importance to improve their electrochemical performance.

Recently, conjugated microporous polymers (CMP) have attracted considerable interests due to their 3D interlinked porous structure, large Brunauer–Emmett–Teller (BET) specific surface areas and good chemical stability[13-19]. In particular, the CMP have active sites (C≡C bonds) for binding of metallic ions[17]. We believe such special physicochemical properties can be used for design of metal oxide/carbon nanocomposite with uniform metal oxide dispersion as an anode material for LIBs. In our previous studies[19], we have demonstrated a porous hard carbon (PHC) via simple one-step thermolysis of CMP precursors as anode materials for LIBs. The CMP-derived PHC shows not only similar porous structure to CMP, but also exhibits high reversible lithium storage capacity, large rate performance , long cycling life but larger initial irreversible lithium storage capacity. In a continuation of the previous work, here we report the utilization of the CMP-derived PHC to improve the poor cyclic stability of MnO anode and decrease the initial irreversible lithium storage capacity of PHC. Along this line, the MnO/PHC nanocomposite was prepared by doping the Mn(II) into CMP precursor followed by thermolysis of the precursor. The MnO/PHC anode exhibits superior lithium storage performances and long cycling life, which may provide an opportunity for fabrication of a novel MnO/porous hard carbon nanocomposite with enhanced lithium storage performance for LIBs.

Experimental

CMP were synthesized from 1,3,5-triethynylbenzene using Pd(II)/Cu(I)-catalyzed homocoupling polymerization. Details have been described in our previous studies[18, 19]. Firstly, $Mn(CH_3COO)_2$ ethanol solution was adsorbed by CMP and then dried at a vacuum drying oven for 1 hours. This step was repeated for several times till the Mn(II) in stoichiometric ratio was totally adsorbed in CMP. (The mole ratio of C≡C/Mn(II) is 1:1). Secondly, the as prepared precursors were calcined at

400 °C for 2 h, and then kept at 700 °C for 4 h under the flow of nitrogen to obtain the MnO/PHC nanocomposite. In order to compare the electrochemical performance of MnO/PHC nanocomposite, the counterpart MnO was also prepared by thermolysis of $Mn(CH_3COO)_2 \cdot 4H_2O$ at the same conditions.

The crystalline structure of MnO/PHC nanocomposite and MnO was determinded by a Rigaku RINT2000 diffractometer with Cu K_α radiation (λ= 0.154 nm). The morphology of the two samples was then observed by a scanning electron microscope (SEM JSM-6701F). The microstructure of MnO/PHC nanocomposite was further determined by a transmission electron microscope (TEM JSM-2100F). The porous properties of MnO/PHC nanocomposite and MnO were evaluated by performing nitrogen adsorption analyses at 77 K using a micromeritics ASAP 2020 apparatus. The carbon content of the MnO/PHC nanocomposite was further determined by an elemental analysis instrument (Elementar Analysensysteme GmbH).

CR2032 coin cells, including a working electrode (MnO/PHC electrode or MnO electrode) and a lithium metal counter electrode separated by a celgard 2400 microporous polypropylene separator, were assembled in a glove box filled with Ar with humidity less than 5 ppm. All the electrodes consist of 75% active materials, 15% Super-P carbon black, and 10% aqueous LA132 binder (Chengdu Chengdu Indigo power sources CO., Ltd.). The coin cells were then discharge/charged between 0 and 3V at room temperature (25°C) using a CT2001A LAND battery testing system (Wuhan LAND Electronics Co., Ltd.). The cyclic voltammetry of the fresh cells were measured by a CHI660D electrochemical workstation (Shanghai Chenhua Instruments Co., China).

Results and discussion

The X-ray diffraction (XRD) patterns of the MnO/PHC nanocomposite and MnO are shown in Fig. 1. MnO in both samples are in face centered cubic phase (JCPDS, 07-0230). Both samples have a few Mn_2O_3 impurity. In addition, MnO/PHC nanocomopsite exhibits a broad and low diffraction intensity peaks in the range of 20-30°, is likely associated with the presence of amorphous carbon, which is originated from the decomposition of the CMP[11, 20-21]. The PHC content in the MnO/PHC nanocomposite was found to be 23.5% by an elemental analyzer, further reflecting the existence of PHC in the nanocomposite.

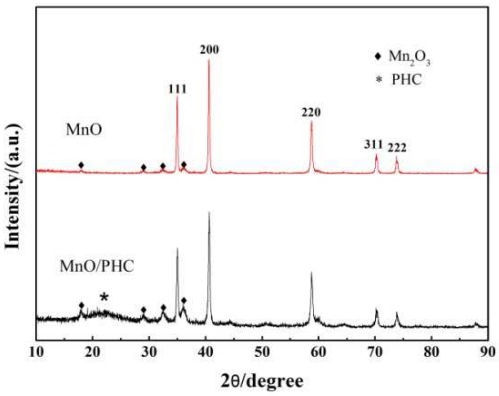

Fig. 1 XRD patterns of MnO/PHC nanocomposite and MnO.

Shown in Fig. 2 are the SEM images of the MnO/PHC nanocomposite and MnO. The MnO/PHC nanocomposite is the aggregates of spherical nanoparticles with a particle size of 30-70 nm (Fig. 2a and Fig. 2b), which are very similar to the PHC (Fig S1 in the supporting information). However, MnO is the aggregates of nanoparticles with a particle size of 30-200 nm (Fig. 2a and Fig. 2b) and most of the particles have a size of 120-200 nm. The morphology of MnO particles is irregular shapes like spheres and flakes. Thus, we can assume that MnO nano crystals should be filled in the pores of PHC.

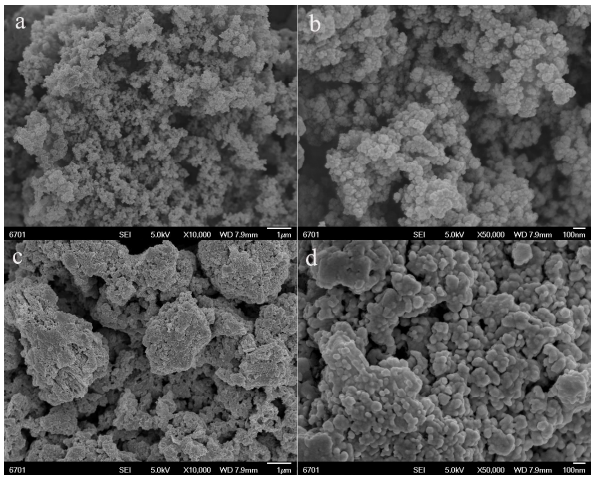

Fig. 2 SEM images of MnO/PHC nanocomposite (a) scale bar: 1 μm and (b) scale bar: 100 nm. SEM images of MnO (c) scale bar: 1 μm and (d) scale bar: 100 nm

Fig. 3 is the TEM image of MnO and MnO/PHC nanocomposite. Fig. 3a is the TEM image of MnO/PHC nanocomposite. Most of the MnO nano crystals about 15 nm are uniformly dispersed in the PHC matrix. The size of MnO nano crystals is obviously smaller than that of PHC nanoparticles (30-70 nm, Fig. S1, ESI†), which indicates MnO nano crystals are located inside the PHC nanoparticles. Fig. 3b is the high resolution TEM image, which shows a lattice structures of MnO (dark region) embedded in the amorphous PHC. Fig. 3c is the TEM image of MnO. The size of MnO particles is in the range of 100-200 nm, which is greatly consistent with SEM results. Fig. 3d is the high resolution TEM image, which clearly shows the lattice structures of MnO.

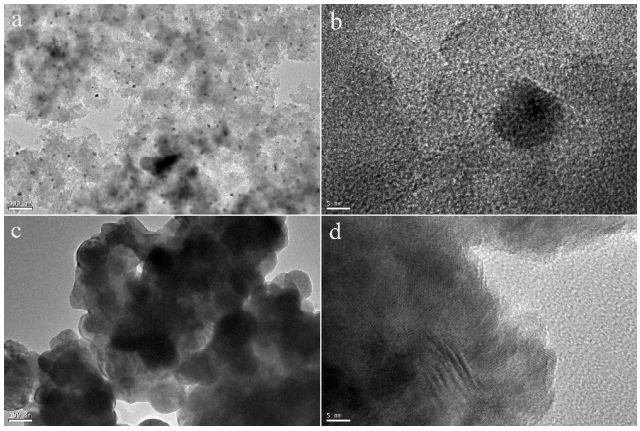

Fig. 3 TEM images of MnO/PHC nanocomposite (a) scale bar: 100 nm and (b) sacle bar: 5 nm. TEM images of MnO (c) scale bar: 100 nm and (d) sacle bar: 5 nm.

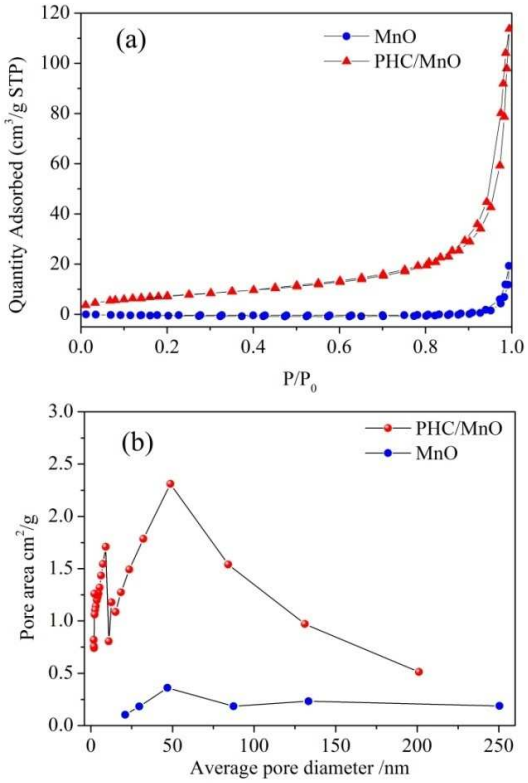

Fig. 4 (a) Nitrogen adsorption–desorption isotherms of MnO/PHC nanocomposite and MnO. (b) Pore distribution of MnO/PHC nanocomposite and MnO.

Nitrogen adsorption analyses were also used to evaluate the porous properties of the MnO/PHC nanocomposite and MnO at 77 K. They both display an isotherm between type II and IV as illustrated in Fig. 4a. The pore volume was estimated from the amount of nitrogen adsorbed at a relative pressure of $P/P_0 = 0.99$ and that of MnO/PHC nanocomposite and MnO are 0.09 $cm^3\ g^{-1}$ and 0.01 $cm^3\ g^{-1}$, respectively. The as prepared MnO/PHC nanocomposite and MnO exhibit a BET surface area of 27.3 $m^2\ g^{-1}$ and 0.03 $m^2\ g^{-1}$, respectively. The pore volume and BET surface area of PHC are 0.77 $cm^3\ g^{-1}$ and 575 $m^2\ g^{-1}$, which have been shown in our previous work[18]. Compared to the PHC, the pore volume and BET surface area are greatly decreased. According to the mass ratio of the MnO/PHC nanocomposite, the conventional mixture of MnO and PHC should have a BET surface area of 135.15 $m^2\ g^{-1}$, which is greatly larger than that of the MnO/PHC nanocomposite (27.3 $m^2\ g^{-1}$). The phenomenon indicates that MnO nano crystals are dispersed in the PHC matrix and fill the PHC pores, which is very accord with the SEM and TEM results. Generally for porous carbon, high surface area results in high initial irreversible capacity[19]. Thus, the decreased surface area is in favor of the decreasing the high initial irreversible capacity. Fig. 4b shows the pore distributions of MnO/PHC nanocomposite and MnO. The former has two main pore distributions (9 nm and 54 nm) and the later has only one pore distributions (48 nm). The pore distributions of 9 nm are attributed to the PHC in the MnO/PHC nanocomposite. The nitrogen adsorption-desorption isotherm and pore size distribution of PHC is shown in Fig. S2 (see ESI†). Compared the pore size distributions of PHC, the pores less than 3 nm are not observed, which implies that these pores may be filled or blocked by MnO nanoparticles.

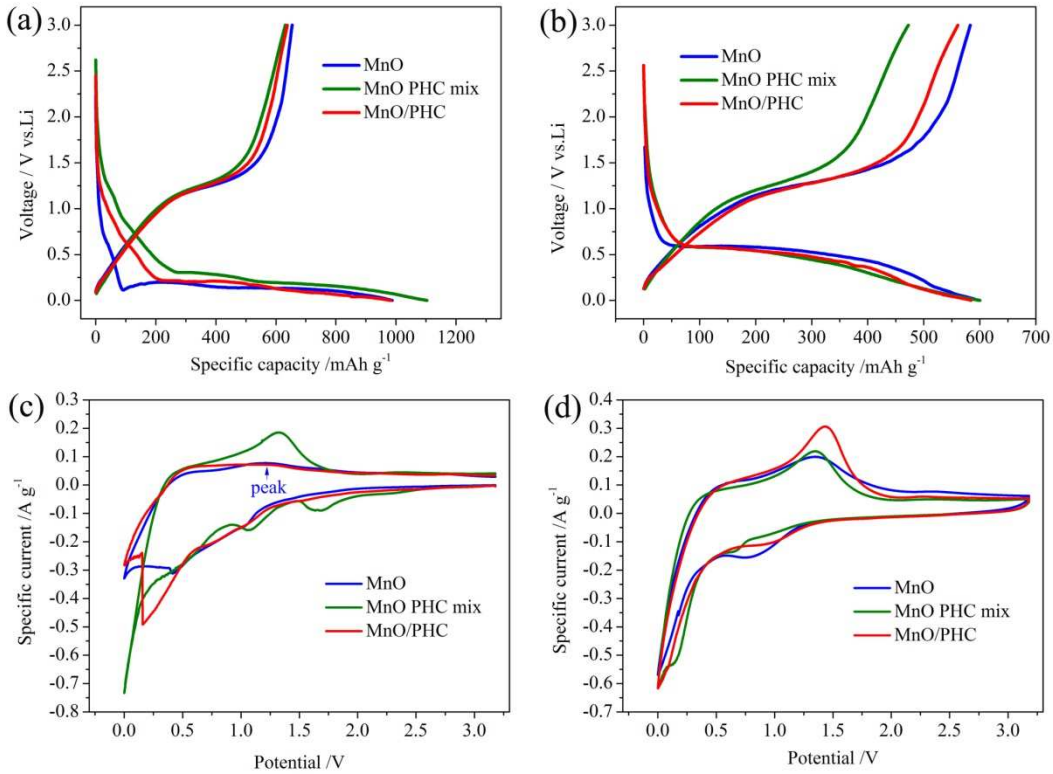

Fig. 5 Charge/discharge curves of MnO, MnO/PHC nanocomposite and MnO PHC mix (a) Initial and (b) Third. Cyclic voltammetry curves of MnO, MnO/PHC nanocomposite and MnO PHC mix (c) Initial and (d) Second.

Initial discharge/charge (lithiation/delithiation) curves of the MnO, MnO/PHC nanocomposite and conventional MnO PHC mixture (MnO PHC mix) are shown in Fig. 5a, b. The discharge/charge current rate is 0.2 C. A defined conversion 0.1 V (vs. Li^+/Li) plateau is observed for both the MnO electrode and MnO/PHC electrode in the first discharge process. The 0.1 V plateau of the MnO electrode begins at 90 mAh g^{-1}, which is in great accordance with previous reports[5]. However, that of MnO/PHC electrode begins at 200 mAh g^{-1} due to the fact that PHC has no discharge voltage plateau[19]. MnO exhibits an initial discharge capacity of 987.7 mAh g^{-1} and a charge capacity of 653.9 mAh g^{-1}. MnO/PHC nanocomposite exhibits an initial discharge capacity of 983.2 mAh g^{-1} and a charge capacity of 638.0 mAh g^{-1}. MnO PHC mix exhibits an initial discharge capacity of 1103.7 mAh g^{-1} and a charge capacity of 631.3 mAh g^{-1}. The first cycle efficiency of MnO PHC mix is 57%, which is clearly lower than that MnO/PHC nanocomposite (65%) and MnO (66%).The results is consistent with the BET results that decreased surface area is in favor of the decreasing the high initial irreversible capacity. As shown in Fig. 5b, the specific capacity of MnO PHC mixture is nearly as same as that of MnO/PHC and MnO, but it still has a much lower charge capcity in the third discharge/charge cycle. The discharge curves and charge curves of MnO/PHC electrode is nearly consistent with that of MnO electrode, but the capacity of former is a little lower than that of the latter. The results means that 23.5% PHC has little negative factor on the voltage hysteresis of MnO although the PHC has no discharge/charge voltage plateau.

Fig. 5c is the first cyclic voltammetry (CV) curves in the range of 0-3.18 V with a scan rate of 0.5 mV s^{-1}. From the increased cathodic current, it can be assumed that the solid electrolyte interphase (SEI) formation[22] starts to take place at 1.4 V. MnO electrode has a wide reduction peak between 0.01 V to 0.5 V (two small peaks at 0.01 V and 0.4 V), while, MnO/PHC electrode has two peaks at 0.01 V and 0.2 V. The result is consistent with the initial discharge curves that MnO electrode firstly reach discharge voltage plateau. MnO PHC mix eletrode shows clear different CV curves. The sharp peaks at 0.01 V is the typical cathodic peaks of PHC, which is shown in our previous study[19]. As shown in Fig. 5d, the second CV cycles indicates that the oxide peak voltage of MnO/PHC electrode is larger than that of MnO electrode and MnO PHC mix electrode. It indicates that MnO/PHC electrode has the best performance.

Because of the poor cycling performance of MnO PHC mix, it can not deliver relatively high spcific capacity after 10 cycles at 0.2 C. Therefore, we only compare electrochemical performance of MnO and MnO/PHC in the following text. Fig. 6a is the discharge/charge capacity of MnO and MnO/PHC electrodes cycled at enhanced rates. At lower current rates (less than 3 C), MnO electrode shows a little higher discharge/charge capacity. When the current rate is equal or greater than 5 C, MnO/PHC electrode exhibits obviously higher discharge/charge capacities. The phenomenon is strange and the reason might be as follows. MnO has large specific capacity and can deliver its capacity at lower current rates. However, MnO can not exhibit high specific capacity because of its limited surface area, which can not adsorb enough electrolytes, allowing the fast electrochemical reactions. Once upon decreasing the rate from 20 C to 0.2 C, MnO/PHC

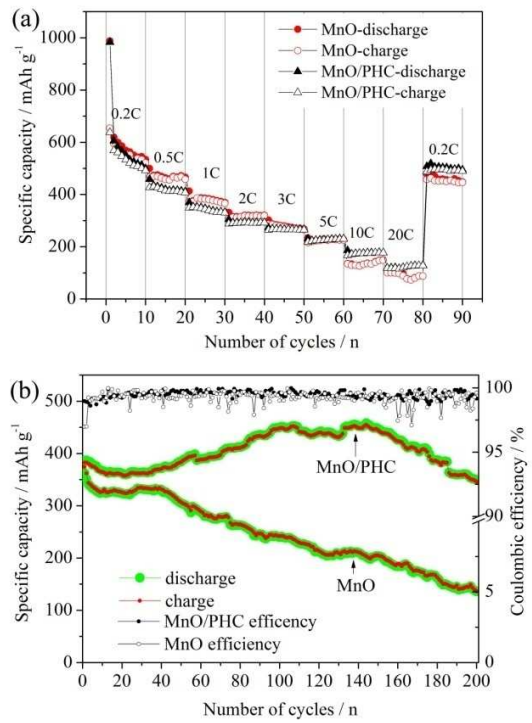

Fig. 6 (a) Rate performance of the MnO/PHC and MnO electrode. (b) Cycling performance of the MnO/PHC and MnO electrode at a charge/discharge rate of 1 C for 200 cycles.

electrode exhibits higher discharge/charge capacities, which indicates that MnO/PHC electrode has large rate discharge/charge capability and good cycling performance. After the rate performance test, the two electrodes were further discharge-charged at a rate of 1 C for 200 cycles and the result is shown in Fig. 6b. The discharge capacity of MnO/PHC electrode roughly increases to 456.0 mAh g^{-1} at 145 cycles and then decrease to 348.7 mAh g^{-1}. Its first discharge capacity is 382.8 mAh g^{-1} and then its capacity retention ratio is 91.1%. The charge/discharge cycles and current density in our work are much more than that in reference[9] and thus the cycling performance is superior to common MnO/C composites. The discharge capacity of MnO electrode mainly decreases from 1 to 200 cycles. Its first and 200th discharge capacity are 362.8 mAh g^{-1} and 135.7 mAh g^{-1}, respectively. The capacity retention ratio of MnO electrode is 37.4%. MnO/PHC electrode shows excellent cycling performance compared to the MnO electrode. It indicates CMP-derived PHC can greatly enhance the cyclic stability of MnO.

In order to further evaluate the cycling performance of MnO/PHC electrode, two another cells were assembled and discharge/charged between 0 and 3 V at 0.2 C for three times to activate the electrodes. Then, the two cells were charge-discharged at 2 C for 300 cycles. The results are shown in Fig. 7. The second charge (delithiation) capacity was chosen as the initial capacity. As illustrated, the initial capacity of MnO/PHC electrode is 395.5 mAh g^{-1}, 85.0% of the initial discharge capacity after 300 cycles is remained, whereas that of the MnO electrode is 393.5 mAh g^{-1}, only 8.2% of the initial discharge capacity after 150 cycles is remained. Clearly, MnO/PHC electrode exhibits the excellent cycling performance.

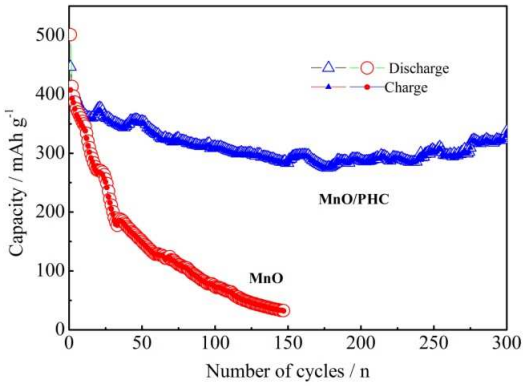

Fig. 7 Comparison of the cycling performance of the MnO/PHC and MnO electrode at a charge/discharge rate of 2 C for 300 cycles.

Conclusions

MnO/PHC nanocomposite has been prepared by doping the Mn(II) into CMP precursor followed by thermolysis of the precursor, which shows improved rate performance and long cycling performance compared to that of MnO. The special physicochemical properties of CMP make it possible to bind metal ions which can be used for preparation of various MOx/carbon nanocomposite with good metal oxide dispersion only by a simple thermolysis process. Those promising prospect may open a new way for the rational design of MO_x/porous carbons as anode materials for high performance LIBs.

Acknowledgements

This research was supported by the National Nature Science Foundation of China (No. 51263012, 51262019, 21466020), Gansu Provincial Science Fund for Distinguished Young Scholars (Grant No. 1308RJDA012).

Notes and references

a School of Petrochemical Engineering, Lanzhou University of Technology, Lanzhou 730050, China. Email: lian2010@lut.cn (A. Li*)* .
b School of Material Science and Engineering, Lanzhou University of Technology, Lanzhou 730050, China

† Electronic Supplementary Information (ESI) available: [details of any supplementary information available should be included here]. See DOI: 10.1039/b000000x/

‡ Footnotes should appear here. These might include comments relevant to but not central to the matter under discussion, limited experimental and spectral data, and crystallographic data.

1. P. Poizot, S. Laruelle, S. Grugeon, L. Dupont, J. M. Tarascon, *Nature*, 2000, **407**, 496-499.
2. H. Li, P. Balaya, J. Maier, *J. Electrochem. Soc*, 2004, **151**, A1878-A1885.
3. X. Q. Yu, Y. He, J. P. Sun, K. Tang, H. Li, L. Q. Chen, X. J. Huang, *Electrochem. Commun*, 2009, **11**, 791-794.
4. K. F. Zhong, X. Xia, B. Zhang, H. Li, Z. X. Wang, L. Q. Chen, *J. Power Sources*, 2010, **195**, 3300-3308.
5. Y. J. Mai, D. Zhang, Y. Q. Qiao, C. D. Gu, X. L. Wang, J. P. Tu, *J. Power Sources*, 2012, **216**, 201-207.
6. X. H. Huang, J. P. Tu, C. Q. Zhang, J. Y. Xiang, *Electrochem. Commun*, 2007, **9**, 1180-1184.
7. J. Y. Xiang, J. P. Tu, Y. F. Yuan, X. L. Wang, X. H. Huang, Z. Y. Zeng, *Electrochim.Acta*, 2009, **54**, 1160-1165.
8. Y. M. Liu, X. Y. Zhao, F. Li, D. G. Xia, *Electrochim. Acta*, 2011, **56**, 6448-6452.
9. J. Liu, Q. M. Pan, *Electrochem. Solid State Lett*, 2010, **13**, A139-A142.
10. Y. L. Ding, C. Y. Wu, H. M. Yu, J. Xie, G. S. Cao, T. J. Zhu, X. B. Zhao, Y. W. Zeng, *Electrochim. Acta*, 2011, **56**, 5844-5848.
11. B. Sun, Z. X. Chen, H. S. Kim, H. Ahn, G. X. Wang, *J. Power Sources*, 2011, **196**, 3346-3349.
12. C. T. Hsieh, C. Y. Lin, J. Y. Lin, *Electrochim. Acta*, 2011, **56**, 8861-8867.
13. A. Thomas, Angew. Chem., *Int. Ed.*, 2010, **49**, 8328-8344.
14. J. Weber, A. Thomas, *J. Am. Chem. Soc.*, 2008, **130**, 6334-6335.
15. Y. Xie, T. T. Zhang, X. H. Liu, K. Zou, W. Q. Deng, *Nat. Commun*, 2013, **4**, 1960-1964.
16. J. X. Jiang, F. Su, A. Trewin, C. D. Wood, H. Niu, J. T. A. Jones,Y. Z. Khimyak, A. I. Cooper, *J. Am. Chem. Soc.*, 2008, **130**, 7710-7720.
17. A. Li, R. F. Lu, Y. Wang, X. Wang, K. L. Han, W. Q. Deng, Angew. Chem., *Int. Ed.*, 2010, **49**, 3330-3333.
18. A. Li, H. X. Sun, D. Z. Tan, W. J. Fan, S. H. Wen, X. J. Qing, G. X. Li, S. Y. Li, W. Q. Deng, *Energy Environ. Sci.*, 2011, **4**, 2062-2065.
19. Q. Zhang, H. Sun, X. Wang, Z. Zhu, W. Liang, A. Li, S. Wen, W. Deng, *Energy Technol.*, 2013, **1**, 721-725.
20. Z. Yang, Y. Xia, R. Mokaya, *J. Am. Chem. Soc.*, 2007, **129**, 1673-1679.
21. H. Sun, A. Li, Z. Zhu, W. Liang, X. Zhao, P. La, W. Deng, *ChemSusChem.*, 2013, **6**, 1057-1062.
22. P. Verma, P. Maire, P. Novak, *Electrochim. Acta*, 2010, **55**, 6332-6341.